

Inhibition of Monoamine Oxidase-B by 5*H*-Indeno[1,2-*c*]pyridazines: Biological Activities, Quantitative Structure–Activity Relationships (QSARs) and 3D-QSARs

Silvia Kneubühler,[†] Ulrike Thull,[†] Cosimo Altomare,[‡] Vincenzo Carta,[‡] Patrick Gaillard,[†] Pierre-Alain Carrupt,[†] Angelo Carotti,^{*,‡} and Bernard Testa^{*,†}

Institut de Chimie Thérapeutique, Section de Pharmacie, Université de Lausanne, CH-1015 Lausanne-Dorigny, Switzerland, and Dipartimento Farmacochimico, Università di Bari, Via Orabona 4, I-70126 Bari, Italy

Received March 7, 1995[⊗]

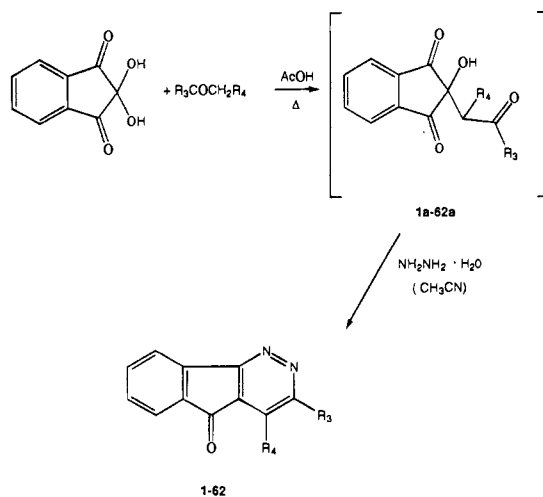
A large series (66 compounds) of indeno[1,2-*c*]pyridazin-5-ones (IPs) were synthesized and tested on their monoamine oxidase-A (MAO-A) and MAO-B inhibitory activity. All of the tested compounds acted preferentially on MAO-B displaying weak (nonmeasurable IC₅₀ values) to high (submicromolar IC₅₀ values) activities. The most active compound was *p*-CF₃-3-phenyl-IP (IC₅₀ = 90 nM). Multiple linear regression analysis of the substituted 3-phenyl-IPs yielded good statistical results ($q^2 = 0.74$; $r^2 = 0.86$) and showed the importance of lipophilic, electronic, and steric properties of the substituents in determining inhibitory potency. Various comparative molecular field analysis studies were performed with different alignments and including the molecular lipophilicity potential. This led to a model including the steric, electrostatic and lipophilicity fields and having a good predictive value ($q^2 = 0.75$; $r^2 = 0.93$).

Introduction

Monoamine oxidase (MAO, EC 1.4.3.4.) is a flavin adenine dinucleotide (FAD)-containing flavoenzyme existing as two isozymes (MAO-A and MAO-B) and playing a key role in the regulation of various physiological amines. This enzyme is also a target for therapeutic agents, MAO-A inhibitors being used as antidepressants, while MAO-B inhibitors like selegiline coadministered with L-DOPA are of interest in the treatment of Parkinson's disease. Irreversible, mechanism-based inactivators of MAO are considered obsolete due to severe side effects such as hepatotoxicity and the well-known "cheese effect". Based on a better understanding of the biochemical and catalytic properties of MAO, recent research efforts have focused on selective and reversible inhibitors of MAO-A or MAO-B.^{1–8}

Pyridazine derivatives are currently an object of sustained interest due to the vast range of their potential activities as chemotherapeutics, antithrombotics, cardiovascular agents, antisecretory and antiulcer agents, analgetic and antiinflammatory agents, and central nervous system (CNS) stimulants or depressants.^{9,10} In a previous paper, we reported the synthesis and activity of a series of novel 5*H*-indeno[1,2-*c*]pyridazin-5-ones (IPs) acting as competitive inhibitors of MAO and mainly MAO-B.^{11–13} Such IPs have a structural analogy (the endocyclic N–N functionality) with 2-aryl-1,3,4-oxadiazines and 5-aryl-1,3,4-oxadiazoles which have been described as selective and competitive MAO-B inhibitors.^{10,14,15} In order to improve the MAO inhibitory activity of IPs and gain an understanding of their structure–activity relationships, we designed, prepared, and tested a large congeneric series of 3- and 4-substituted indeno[1,2-*c*]pyridazine derivatives. Their synthesis, MAO inhibitory activities, and structure–activity relationships are described in this paper. The

Scheme 1. General Synthetic Method Used in This Work



very good quantitative structure–activity relationship (QSAR) and 3D-QSAR models obtained afford interesting insights into the topography of the MAO-B enzymatic site.

Results and Discussion

Chemistry. Compounds 1–62 were prepared from ninhydrin and the adequate ketone according to the reaction pathway reported in Scheme 1. In most cases the synthesis was carried out by a one-pot procedure. In the case of very low yields or when the intermediate aldol adducts 1a–62a precipitated from the reaction mixture, a classical two-step synthesis was adopted. The preparation of the condensed pyridazines 4, 6, 8–10, 12, 15, 17–25, 28–30, 33, 34, 39, 41, 43–45, 47, 53, and 55–58 has already been described by some of us.^{11,12} Reaction yields, physicochemical properties, and spectral data of the newly synthesized condensed pyridazines are given in the Experimental Section, and those of the isolated aldol adducts are reported in Table 1.

[†] Université de Lausanne.

[‡] Università di Bari.

[⊗] Abstract published in *Advance ACS Abstracts*, August 1, 1995.

Table 1. Physicochemical and Spectroscopic Data of Intermediate Aldol Adducts

compd	yield (%)	mp (°C) (cryst solv) ^a	IR (cm ⁻¹)	¹ H-NMR (90 MHz, DMSO- <i>d</i> ₆) δ
22a	42	184–5 (A)	3120, 1750, 1725, 1710	8.02 (s, 4H), 3.48 (s, 2H), 2.77 (t, 2H, <i>J</i> = 6.5 Hz), 2.38 (t, 2H, <i>J</i> = 6.5 Hz), COOH not detected ^b
54a	70	187–9 dec (A)	3380, 2240, 1755, 1715, 1675	8.07 (s, 8H), 6.90 (s, 1H, D ₂ O exchange), 4.01 (s, 2H)
59a	50	160–1 (D)	3400, 1750, 1710, 1680, 1670	8.06 (s, 8H), 6.85 (s, 1H, D ₂ O exchange), 3.98 (s, 2H), 2.60 (s, 3H)
60a	60	211–2 (A)	3440, 3340, 1750, 1730, 1720, 1660, 1655	10.28 (s, 1H, D ₂ O exchange), 8.03 (s, 4H), 7.85 (d, 2H, <i>J</i> = 9 Hz), 7.68 (d, 2H, <i>J</i> = 9 Hz), 6.77 (s, 1H, D ₂ O exchange), 3.88 (s, 2H), 2.07 (s, 3H)
61a	65	103–4 (E)	3425, 1750, 1710, 1705, 1665	8.04 (s, 4H), 7.87 (d, 2H, <i>J</i> = 9 Hz), 6.98 (d, 2H, <i>J</i> = 9 Hz), 6.78 (s, 1H, D ₂ O exchange), 4.03 (t, 2H, <i>J</i> = 7.5 Hz), 3.88 (s, 2H), 1.2–1.8 (m, 4H), 0.89 (t, 3H, <i>J</i> = 6.5 Hz)
62a	30	181–2 (B)	3430, 1750, 1710, 1660	8.01 (s, 4H), 7.67 (d, 2H, <i>J</i> = 9 Hz), 6.85 (d, 2H, <i>J</i> = 9 Hz), 6.68 (s, 1H, D ₂ O exchange), 3.80 (s, 2H), 3.34 (br, 4H), 1.55 (br, 6H)

^a A: ethyl acetate/hexane. B: ethanol. C: CHCl₃/hexane. D: THF/hexane. E: CCl₄. ^b Recorded in acetone-*d*₆.

The 7-methoxyindeno[1,2-*c*]pyridazine derivative **64** was prepared from 5-methoxyninhydrin, 3-(trifluoromethyl)acetophenone, and hydrazine by the one-pot method. Demethylation of **64** to the phenolic derivative **65** was achieved with HBr in acetic acid. Oxidation of compound **12** with CrO₃ and of compound **23** with DDQ afforded the dioxo derivative **13** and indeno[1,2-*c*]cinnolin-11-one (**27**), respectively.

MAO-A and MAO-B Inhibition. Sixty-six compounds were tested for their *in vitro* inhibitory effect on MAO-A and MAO-B. The competitive, reversible MAO inhibitor harman was used as reference for the two isozymes.¹⁶ The compounds are divided into series A where variations are in positions 3 and 4 of the indenopyridazine ring, and series B, which contains mostly 3-(substituted phenyl)indenopyridazines. As shown in Tables 2 (series A) and 3 (series B), the majority of the compounds act preferentially as MAO-B inhibitors with IC₅₀ values in the micro- to submicromolar range. The most potent inhibitor was compound **51** (3-*p*-CF₃-phenyl-IP) with an IC₅₀ value of 90 nM.

At a substrate concentration of 540 μ M instead of 60 μ M, markedly reduced inhibitions were seen for all inhibitors. Preincubating the compounds for 15 or 5 min at the IC₅₀ and at the same substrate concentration made no difference in the degree of inhibition. Thus all the tested compounds seem to act in a reversible and time-independent manner (results not shown).

In series A (Table 2), the unsubstituted compound **1** was already active and selective toward MAO-B. Mono-substitution in position 3 usually led to more active or equipotent compounds (**7**, **12–17**). Irrespective of the 4-substituent, a 3-phenyl substituent was highly favorable to activity (**7**, **9–11**). A surprising result, however, is the poor activity of compound **8** (3-phenyl-4-methyl-IP), since the absence of a 4-substituent or a 4-substituent larger than methyl (benzyl, benzoyl, ethoxycarbonyl; **9–11**) increases activity relative to compound **8**.

It is also interesting to note that a heterocycle in position 3 is unfavorable to activity (**18–21**). An additional ring linked at positions 3 and 4 destroys activity (**24–27**), with the interesting exception of compound **23** which was active toward MAO-A. Several other inhibitors in Table 2 displayed weak inhibitory activity toward MAO-A, but no structural requirements are apparent.

A *trans*-styryl (**15**) or β -naphthyl (**17**) substituent in position 3 increased activity 10-fold compared to the phenyl substituent. However, neither of these two derivatives were chosen as a lead compound for further

optimization due to their poor solubility and to promising preliminary results with *para*-substituted derivatives of compound **7**.¹⁷

The derivative **7** was thus taken as a lead compound and its activity optimized by variously substituting the 3-phenyl ring in the 2', 3', and/or 4' positions (Table 3). Several among these derivatives indeed proved more active than compound **7** toward MAO-B, with the exception of some *ortho*-substituted compounds (**28**, **32**, **55**) and those bearing an amino, acetamido, or carboxylic group (**37**, **38**, **58**, **60**). *Ortho* substitution was regularly an unfavorable feature, as evidence by the fact that a given substituent was more favorable in the *meta* or *para* than in the *ortho* position (compare the regioisomers **29–31**, **32–34**, **39–41**, **43–45**, **49–51**, **55–57**). With the exception of compounds **33** and **47**, *para*-substituted derivatives appeared as slightly more active than the *meta*-substituted analogs. A *p*-CF₃ group (compound **51**) proved the most favorable to activity (200-fold increase relative to the parent compound).

Such preliminary considerations suggest the involvement of steric and electronic factors in influencing MAO-B inhibition by IPs. Furthermore, lipophilicity may also be implicated as deduced from the influence of the OH, CN, and CF₃ substituents.

The compounds in series B are only slightly active (compounds **39–41**, **43–45**) or inactive toward MAO-A. Interestingly, an amino group (compounds **37**, **38**) increases MAO-A inhibitory activity.

In regard to substitution of rings A and B, we already reported¹⁷ that reduction of the 5-carbonyl group of **7** to CH₂ yielded compound **63** which displays comparable MAO-B inhibition, and this suggests that the presence of carbonyl in position 5 (ring B) is not a critical requisite for MAO-B inhibition.

Moreover, in the present study we synthesized compound **64** (3-(trifluoromethyl)-5*H*-indeno[1,2-*c*]pyridazin-5-one) in order to explore direct electronic effects on the pyridazine ring. The resulting MAO-B inhibitory activity (20% of inhibition at maximum solubility, 25 μ M) (Table 4) was much lower than that of the corresponding phenyl homolog **51**. Thus, the phenyl ring at position 3 is important in modulating MAO-B inhibitory activity.

Finally, in order to improve the structural analogy with naturally occurring biogenic amines, compounds **65** and **66** (Table 4) were synthesized bearing methoxy and hydroxy substituents, respectively, in position 7 of the IP nucleus (ring A). Both compounds showed

Table 2. MAO Inhibition Data and CoMFA Prediction for 5*H*-Indeno[1,2-*c*]pyridazin-5-ones (Series A)

compd	R ₃	R ₄	IC ₅₀ ^a (μM)		CoMFA model F7	
			MAO-A	MAO-B	pIC ₅₀	residuals
1	H	H	97.6 ± 8.9	27.5 ± 5.1	4.56	0.40
2	H	phenyl	34.3 ± 3.2	93.7 ± 6.1	4.03	-0.35
3	H	benzyl	<i>c</i>	<i>c</i>		
4	CH ₃	H	> 100 (20%)	74.4 ± 2.5	4.13	-0.06
5	CH ₃	phenyl	<i>c</i>	20.7 ± 1.9	4.68	0.23
6	CH ₃	benzyl	<i>b</i>	83.5 ± 7.8	4.08	-0.06
7	phenyl	H	<i>d</i>	21.0 ± 0.6	4.68	-0.26
8	phenyl	CH ₃	<i>b</i>	> 100 (21%)		
9	phenyl	benzyl	> 10 (13%)	9.5 ± 0.3	5.02	0.06
10	phenyl	benzoyl	<i>e</i>	7.7 ± 0.4	5.11	0.02
11	phenyl	ethoxycarbonyl	> 50 (34%)	5.3 ± 0.2	5.28	0.06
12	benzyl	H	<i>b</i>	30.6 ± 0.3	4.51	0.01
13	benzoyl	H	> 50 (34%)	16.1 ± 0.7	4.80	-0.02
14	phenethyl	H	<i>c</i>	22.4 ± 0.4	4.65	0.09
15	<i>t</i> -CH=CH-phenyl	H	> 1 (12%)	1.5 ± 0.1	5.82	0.13
16	α-naphthyl	H	<i>e</i>	> 5 (26%)		
17	β-naphthyl	H	<i>e</i>	2.18 ± 0.08	5.66	-0.33
18	fur-2'-yl	H	> 50 (27%)	32.5 ± 3.4	4.49	-0.14
19	thien-2'-yl	H	<i>f</i>	<i>f</i>		
20	pyrid-2'-yl	H	<i>d</i>	> 25 (23%)		
21	pyrid-3'-yl	H	> 25 (38%)	> 25 (25%)		
22	CH ₂ CH ₂ COOH	H	<i>b</i>	<i>b</i>		
23			50.5 ± 4.4	<i>b</i>		
24			<i>c</i>	<i>c</i>		
25			<i>c</i>	<i>c</i>		
26			<i>e</i>	<i>e</i>		
27			<i>f</i>	<i>f</i>		

^a Or percent inhibition in parentheses at maximum solubility. No inhibition at maximum solubility: ^b 100 μM, ^c 50 μM, ^d 25 μM, ^e 10 μM, ^f 1 μM.


weaker MAO-B inhibitory activity than the parent compound **50** (Table 4).

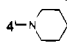
While more structural variations are necessary to derive reliable SARs accounting for the role of rings A and B of the IP nucleus in modulating MAO-B inhibitory activity, substituents at the pyridazine ring appear, at the moment, more important in determining both activity and selectivity.

2D-QSAR Study of MAO-B Inhibition. A classical 2D-QSAR of the 24 3-phenyl-substituted congeners (series B) was carried out using partial least squares (PLS) analysis, cluster analysis (CA), and multilinear regression (MR). In a first step, each substituent was described by 11 parameters, primarily physicochemical in nature. Classical Hammet (σ_m and σ_p) and Swain-Lupton (F and R) constants were used as electronic parameters, and the Hansch constant (π) was used as a descriptor of lipophilicity, while bulkiness was parametrized by the van der Waals volume (V_w). Parameters were taken from standard compilations.^{18,19} Indicator variable (I_{ortho}) was also used to take into account the detrimental effect observed for *ortho* substitution ($I_{ortho} = 1$ for *ortho*-substituted derivatives and 0 for the others). The ¹H-NMR chemical shifts of the aromatic protons in the pyridazinyl and phenyl rings were also used. Since the biologically active conformation of the phenyl ring is unknown, it proved difficult to differenti-

ate between the two *ortho* or the two *meta* positions in the phenyl ring. Thus we defined that *ortho* and *meta* substitution occurs in position 2' and 3' and then consistently considered the chemical shifts of protons 5' and 6'. A preliminary analysis showed that $\Delta\delta_{H5'}$ ($\Delta\delta$ is the difference between the proton chemical shifts of the substituted and unsubstituted X-phenyl derivatives) was reasonably correlated with σ ($r^2 = 0.75$) but that $\Delta\delta_{H6'}$ and $\Delta\delta_{H4}$ were not correlated with electronic parameters due to their strong dependence on conformational effects. Due to this correlation with σ , the chemical shift $\Delta\delta_{H5'}$ was not considered in the statistical analyses.

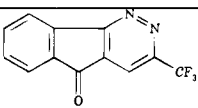
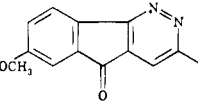
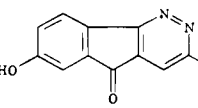
Using the restricted set of 10 structural descriptors, a PLS analysis with a leave-one-out cross-validation procedure afforded a three-component model ($n = 24$; $q^2 = 0.76$; $r^2 = 0.88$; $s = 0.278$; $F = 49$). A cluster analysis of the loadings matrix was then performed in order to identify proximity relations between the 24 compounds in the three-component space. The resulting dendrogram is presented in Figure 1, revealing four groups of compounds and isolated points. The first group (compounds **7**, **33**, **39–42**, **44–48**, **50**, **51**) contains *meta*- and *para*-substituted 3-phenyl-IPs bearing lipophilic ($\pi > 0$) substituents (halogens, trifluoromethyl, methoxy), while the second group (compounds **53**, **54**, **57**, **59**) contains derivatives with hydrophilic ($\pi < 0$) but strongly electron-withdrawing substituents (cyano, ni-

Table 3. MAO Inhibition Data, Physicochemical Parameters Used To Derive Classical QSARs, and CoMFA Predictions for Substituted 3-Phenyl-5H-indeno[1,2-c]pyridazin-5-ones (Series B)


compd	X	IC ₅₀ ^a (μM)		pIC ₅₀	2D-QSAR residuals	CoMFA residuals		Δδ		
		MAO-A	MAO-B			model C7	model F7	H5'	H6'	H4'
7	H	<i>d</i>	21.0 ± 0.6	4.68	-0.62	-0.12	-0.26	0	0	0
28	2'-CH ₃	<i>f</i>	30.9 ± 1.8	4.51	0.08	-0.17	-0.19	-0.15	-0.62	-0.28
29	2'-OH	<i>g</i>	>1 (11%)					-0.51	-0.32	0.26
30	3'-OH	<i>g</i>	>1 (18%)							
31	4'-OH	>50 (28%)	9.9 ± 1.7	5.00	0.18	0	0.06	-0.54	-0.06	-0.04
32	2'-OCH ₃	<i>d</i>	>50 (21%)					-0.42	-0.16	0.16
33	3'-OCH ₃	<i>d</i>	1.6 ± 0.2	5.80	-0.07	0.21	0.24	-0.08	-0.49	0.01
34	4'-OCH ₃	<i>f</i>	3.22 ± 0.04	4.49	-0.06	-0.01	-0.11	-0.51	-0.03	-0.05
35	3',4'-(OCH ₃) ₂	<i>g</i>	<i>g</i>							
36	3'-OCH ₃ , 4'-OH	<i>f</i>	<i>f</i>					-0.05	-0.58	-0.02
37	3'-NH ₂	25.9 ± 3.3	32.3 ± 4.1	4.49	-0.03	-0.04	-0.12	-0.22	-0.71	0.27
38	4'-NH ₂	36.8 ± 2.9	24.7 ± 2.4	4.61	0.24	-0.04	0.04	-0.74	-0.13	-0.07
39	2'-F	>20 (17%)	18.1 ± 1.5	4.74	-0.18	0.07	0.21	-0.31	0.05	0.09
40	3'-F	<i>f</i>	4.2 ± 0.2	5.38	-0.23	-0.06	-0.17	0.04	-0.24	-0.03
41	4'-F	30.6 ± 1.6	0.92 ± 0.06	5.60	0.09	0.09	-0.02	-0.30	0.01	-0.03
42	3',4'-F ₂	<i>g</i>	0.92 ± 0.06	6.04	0.18	-0.07	-0.15	-0.19	-0.29	-0.03
43	2'-Cl	>50 (40%)	15.9 ± 1.0	4.80	0.18	0.10	0.25	-0.01	-0.37	-0.01
44	3'-Cl	>5 (17%)	0.90 ± 0.08	6.05	0.11	0.20	0.20	-0.04	-0.13	-0.02
45	4'-Cl	>5 (30%)	0.92 ± 0.10	6.04	-0.11	0.11	0.20	-0.02	-0.05	-0.02
46	3',5'-Cl ₂	<i>g</i>	0.71 ± 0.02	6.15	-0.42	-0.02	-0.05		-0.10	-0.04
47	3'-Br	<i>g</i>	0.66 ± 0.05	6.18	0.15	0.17	0.20	-0.12	-0.09	-0.02
48	4'-Br	<i>g</i>	1.33 ± 0.09	5.88	-0.43	-0.14	-0.02	0.14	-0.12	-0.02
49	2'-CF ₃	<i>f</i>	<i>f</i>					0.06	-0.28	-0.28
50	3'-CF ₃	>5 (24%)	0.28 ± 0.02	6.55	0.48	-0.09	-0.08	0.14	0.19	0.04
51	4'-CF ₃	<i>g</i>	0.09 ± 0.01	7.05	0.59	-0.17	0.03	0.28	0.13	0.04
52	3',5'-(CF ₃) ₂	<i>g</i>	>2 (15%)						0.49	0.08
53	3'-CN	>10 (17%)	3.7 ± 0.3	5.43	0.07	0.13	0.09	0.14	0.22	0.01
54	4'-CN	<i>e</i>	2.2 ± 0.2	5.66	-0.10	0	0.03	0.31	0.12	0.03
55	2'-NO ₂	<i>c</i>	80.1 ± 4.4	4.10	-0.18	-0.14	-0.36	0.17	-0.34	-0.30
56	3'-NO ₂	<i>g</i>	>0.5 (42%)					0.22	0.40	0.09
57	4'-NO ₂	<i>e</i>	0.50 ± 0.02	6.30	0.29	-0.02	0.15	0.79	0.31	0.09
58	4'-COOH	<i>c</i>	<i>c</i>							
59	4'-COCH ₃	>10 (22%)	1.78 ± 0.09	5.75	-0.20	0	-0.14	0.60	0.12	0.07
60	4'-NHCOCH ₃	>10 (12%)	>10 (9%)					0.17	0	-0.01
61	4'-OC ₄ H ₉	<i>f</i>	<i>f</i>					-0.51	-0.05	-0.06
62	4'- 	<i>g</i>	<i>g</i>					-0.52	-0.07	-0.06
63	H	(31%)	23.4 ± 2.4	4.63			-0.07			

^a Or percent of inhibition in parentheses at maximum solubility. No inhibition at maximum solubility: ^c 100 μM, ^d 50 μM, ^e 25 μM, ^f 10 μM, ^g 1 μM. ^b Different chemical shifts relative to the parent compound 7.

Table 4. MAO Inhibition Data of Compounds 64–66

Cpd.	Structure	IC ₅₀ ^a (μM)	
		MAO-A	MAO-B
64		<i>a</i>	> 25 (20%)
65		<i>b</i>	1.31 ± 0.08
66		<i>b</i>	5.10 ± 0.23

^a No inhibition at maximum solubility: 25 μM, ^b 5 μM.

tro, acetyl). A third group can be observed which contains hydrophilic hydrogen-bond donor substituents (compounds 31, 34, 37, 38) in the *meta* or *para* position. The fourth group contains two *ortho* derivatives (com-

pounds 28, 43). The less active compound 55 (*o*-NO₂) is separated from the previous clusters presumably because the electron-withdrawing capacity of the nitro substituent cannot compensate for the detrimental steric effect of *ortho* substitution.

Although the PLS model is characterized by a good predictive capacity, its interpretation in physicochemical terms remains difficult. We therefore decided to perform a multilinear analysis with the most suitable parameters. The selection of the pertinent structural parameters was done by considering the similarity between parameters and their relative influence on the PLS model. A cluster analysis on the scores matrix of the PLS analysis given in Figure 2 indicates that some structural parameters contain comparable information, namely σ and F or I_{ortho} and V_w2' . Indeed the contribution of some parameters such as R and $\Delta\delta_{H4}$ to the PLS model was very low, respectively 1% and 5%. Thus a stepwise multilinear regression was performed using only six parameters (σ , π , $\Delta\delta_{H4}$, V_w2' , V_w3' , and V_w4').

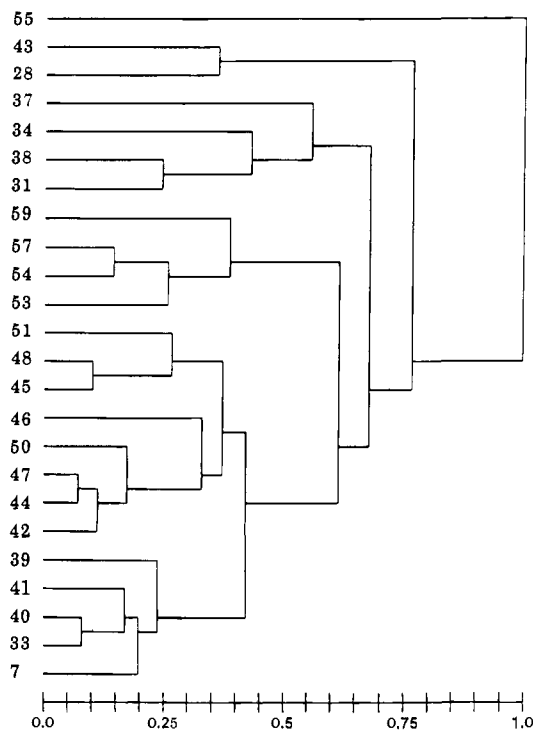


Figure 1. Cluster analysis of the loading matrix of the 24 MAO-B inhibitors in series B. Four groups of compounds emerge, as well as some isolated points.

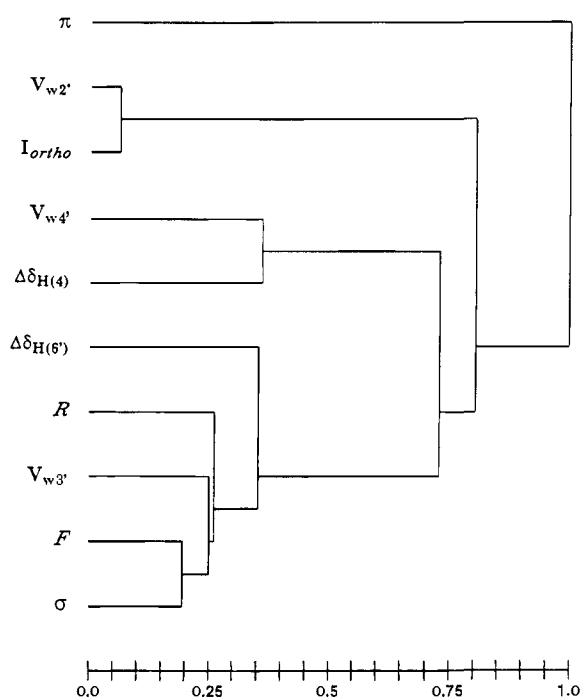


Figure 2. Cluster analysis of the score matrix of the 24 MAO-B inhibitors in series B, revealing which structural parameters contain comparable information, e.g., σ and F or I_{ortho} and $V_{w2'}$.

The stepwise regression analysis retained only four variables to produce eq 1 (95% confidence limits in parentheses):

$$\text{pIC}_{50} = 0.66(\pm 0.36)\sigma + 0.55(\pm 0.23)\pi - 1.25(\pm 0.40)V_{w2'} + 0.31(\pm 0.27)V_{w4'} + 5.51(\pm 0.23) \quad (1)$$

$$n = 24; q^2 = 0.74; r^2 = 0.86; s = 0.31; F = 29$$

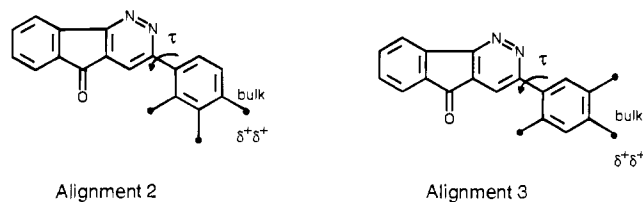


Figure 3. Rules for alignments 2 and 3. The torsion angle τ between the indenopyridazine ring and the phenyl ring in position 3 is fixed at 116° . The difference between alignments 2 and 3 lies in the position of the *meta* substituent; for alignment 2 the *meta* substituent was considered in the 3' position, whereas for alignment 3 it was in the 5' position.

The above results relate MAO-B inhibitory activity mainly to lipophilic and electronic properties of substituents and to a steric negative effect of *ortho* substituents. A small but significant contribution is also noted for the volume of *para* substituents. An extension of the 2D-QSAR to the 39 compounds measured was not possible due to a different pattern of substitution on the 3 and 4 positions of the pyridazinyl ring. A 3D-QSAR study was therefore undertaken.

3D-QSAR Study of MAO-B Inhibition. Since its introduction in 1988,²⁰ comparative molecular field analysis (CoMFA) has proven to be a useful tool in 3D-QSAR studies. In the first step of this study, we used the same compounds as in the above 2D-QSAR investigation (i.e., the 24 compounds of series B, see Table 3). This allowed us to derive a 3D-QSAR model which could readily be compared with eq 1. In a second step, the compounds in series A (Table 2) and series B were pooled together (i.e., 39 compounds with well-defined IC_{50} values) to gain more insights into the structural requirements modulating MAO-B inhibitory activity. The MAO-A data presented here were not suitable to a QSAR analysis due to the limited number of IC_{50} s.

Alignment. The superposition of all compounds is a critical step in any CoMFA study. As a first anchor point the very rigid indeno[1,2-*c*]pyridazine rings were superimposed atom by atom. Then, we derived different alignments for several substituent orientations. No further alignment was necessary if the conformation of minimal energy was used, otherwise the substituents were aligned according to (a) the angle τ between the indenopyridazine ring and the phenyl ring in position 3, (b) the topology of the substituents on the phenyl ring, and (c) the orientation of these substituents. For the torsion angle τ between the indenopyridazine ring and the 3 substituent, a conformational analysis showed the existence of two zones (75° – 140° , 260° – 320°) of low energy within which the angle could be modified without significant difference in energy.

Three alignments were retained (because of their maximal predictive power) among the many ones tested. For alignment 1, the indeno[1,2-*c*]pyridazine rings were superimposed with their substituents in the minimum-energy conformation. The alignment rules for alignments 2 and 3, which take into account the unknown orientation of *ortho* and *meta* substituents, are presented in Figure 3. The torsion angle τ between the indenopyridazine ring and the phenyl ring in position 3 was kept at the average minimum value of 116° calculated for all the *ortho*-substituted compounds. We also derived a model based on alignment 3 and defined by the field fit option, but its quality was low (results not shown).

Table 5. Statistical Results of CoMFA Analyses of 24 Indeno[1,2-*c*]pyridazines (Series B)

model	q^2 ^b	N^c	r^2	relative contribution		
				ste	ele	lipo
alignment 1 ^a						
A1	steric field (ste)	0.26	1			
A2	electrostatic field (ele)	0.26	1			
A3	lipophilic field (lipo)	0.30	4			
A4	ste and ele	0.42	2	0.67	0.38	0.62
A5	ste and lipo	0.69	3	0.90	0.62	0.38
A6	ele and lipo	0.57	1	0.78		0.64
A7	ele, ste and lipo	0.83	4	0.98	0.36	0.37
alignment 2 ^d						
B1	ste	0.27	2			
B2	ele	0.40	4			
B3	lipo	0.20	2			
B4	ste and ele	0.48	2	0.77	0.44	0.56
B5	ste and lipo	0.64	2	0.87	0.65	0.35
B6	ele and lipo	0.78	4	0.94		0.62
B7	ele, ste, and lipo	0.84	4	0.99	0.37	0.35
alignment 3 ^d						
C1	ste	0.23	2			
C2	ele	0.30	3			
C3	lipo	0.35	3			
C4	ste and ele	0.50	2	0.78	0.45	0.55
C5	ste and lipo	0.64	3	0.92	0.61	0.39
C6	ele and lipo	0.63	4	0.92		0.68
C7	ele, ste, and lipo	0.84	3	0.98	0.36	0.36

^a The indenopyridazine rings were superimposed with their substituents in the minimum energy conformation. ^b Cross-validated correlation coefficient. ^c Optimal number of principal components used for the final analysis. ^d See Figure 3.

3D-QSAR of Series B (24 Compounds). The statistical results obtained with the three alignments are presented in Table 5. With each field separately, no good statistical results were obtained ($q^2 \leq 0.4$). In contrast, models incorporating two fields showed a significant improvement, with the lipophilicity field making an important contribution (models A5, A6, B5, B6, C5, C6) relative to the combined electrostatic and steric fields (models A4, B4, C4). However, the best models were obtained by combining the three fields (electrostatic, steric, lipophilic) (A7, B7, C7), with q^2 increasing by about 0.2. It should also be noted that the three alignments gave almost the same model with a identical predictive quality ($q^2 = 0.83, 0.84,$ and 0.84 for models A7, B7 and C7, respectively). From a statistical viewpoint, model C7 is slightly better than the other two since it is based on a smaller number of components. Thus the different alignments influenced only slightly the statistical results but obviously had a large influence on the graphical results, perhaps suggesting a certain flexibility of the active site.

Indeed the graphical representations of model C7 (Figure 4a) show that substitution in the *meta* or *para* position produces a sterically favorable (green) contribution, whereas substitution in the *ortho* position is sterically unfavorable (red) probably due to steric hindrance. The electrostatic contributions consist mainly (a) in an important magenta zone near the *meta* and *para* positions of the 3-phenyl ring where high electron density is favorable to activity and (b) an important white zone near the bond between the aromatic carbon and the *para* substituent where electron deficiency is favorable to activity (Figure 4a). The statistical results of the lipophilic field reveal only lipophilic (yellow) zones favorable for MAO-B inhibitory activity near the *meta* and *para* substituents.

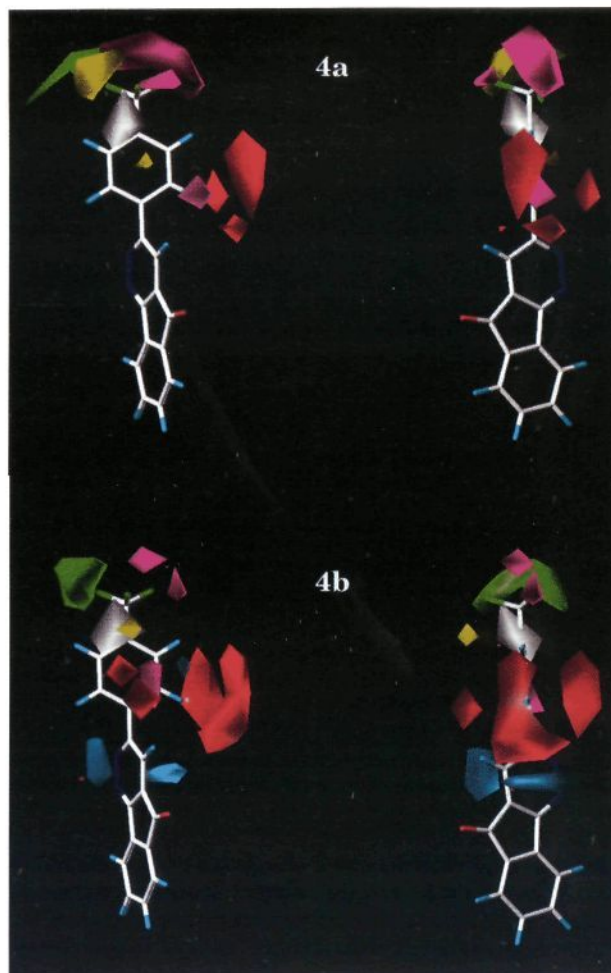


Figure 4. Pictorial representation of 3D-QSAR models. The color code is as follows: sterically favorable and unfavorable influences, green and red zones, respectively; favorable influence of high electron density and deficiency, magenta and white zones, respectively; favorable influence of lipophilic and hydrophilic (polar) groups, yellow and cyan zones, respectively. (a) Model C7 for the 24 MAO-B inhibitors of series B. Substitution in the *meta* and/or *para* position has a favorable steric contribution, whereas substitution in the *ortho* position is sterically unfavorable. The important magenta zone near the *meta* and *para* positions indicates that a high electron density is favorable for activity, whereas electron deficiency is favorable between the aromatic carbon atom in the 4' position and the *para* substituent. Moreover lipophilic substituents in the *meta* and *para* positions are favorable for activity. Contour levels: steric field, 20% red, 75% green; electrostatic field, 20% magenta, 85% white; lipophilic field, 0% cyan, 85% yellow. (b) Model F7 for the 39 MAO-B inhibitors in series A plus B. A bulky substituent in the *para* and/or *meta* position can make a favorable contribution, whereas *ortho* substitution is unfavorable. Electron-withdrawing substituents in the *para* and/or *meta* position produce favorable electron-rich and electron-poor zones. Hydrophilic substituents in position 4 appear to be favorable for activity. Contour levels: steric field, 20% red, 80% green; electrostatic field, 15% magenta, 85% white; lipophilic field, 5% cyan, 85% yellow.

As explained in the Experimental Section, compounds **16** and **56** were taken as the test set. Using model C7, the IC₅₀ predictions for compound **16** (pIC₅₀est_{im} = 4.85/pIC₅₀pred = 4.87) and compound **56** (pIC₅₀est_{im} = 6.16/pIC₅₀pred = 5.88) were quite satisfactory.

Comparison of QSAR and CoMFA Models for Series B (24 Compounds). This comparison leads to

Table 6. Statistical Results of CoMFA Analyses of 39 Indeno[1,2-*c*]pyridazines (series A and B)

model		q^2	N^c	r^2	relative contribution		
					ste	ele	lipo
alignment 1 ^a							
D1	steric field (ste)	0.49	3	0.72			
D2	electrostatic field (ele)	0.37	6				
D3	lipophilic field (lipo)	0.50	1	0.61			
D4	ele and ste	0.59	2	0.78	0.48	0.52	-
D5	ste and lipo	0.67	2	0.82	0.56	-	0.44
D6	ele and lipo	0.65	1	0.78	-	0.53	0.47
D7	ele, ste, and lipo	0.78	3	0.94	0.28	0.37	0.35
alignment 2 ^d							
E1	ste	0.45	7	0.86			
E2	ele	0.35	2				
E3	lipo	0.43	3	0.77			
E4	ele and ste	0.55	2	0.76	0.40	0.60	
E5	ste and lipo	0.71	3	0.92	0.46		0.54
E6	ele and lipo	0.49	4	0.86		0.54	0.46
E7	ele, ste, and lipo	0.70	3	0.91	0.22	0.43	0.35
alignment 3 ^d							
F1	ste	0.39	2				
F2	ele	0.36	3				
F3	lipo	0.46	1	0.57			
F4	ele and ste	0.60	3	0.84	0.46	0.54	
F5	ste and lipo	0.55	2	0.75	0.57		0.43
F6	ele and lipo	0.65	2	0.87		0.49	0.51
F7	ele, ste, and lipo	0.75	3	0.93	0.27	0.41	0.32

^{a-d} See Table 5.

the following conclusions. (1) Ortho effect: The detrimental effect of *ortho* substitution found in the classical QSAR study and expressed by the structural parameter V_w2' is clearly attributed in the CoMFA study to a corresponding region of steric hindrance. (2) Steric and lipophilicity parameters: The favorable influence on activity noted in the QSAR study for the hydrophobic constant π and the volume of *para* substituents is also found in the CoMFA models. Indeed, increased activity is associated with a favorable steric zone (green in the figure) near the *para* position and with a favorable lipophilic zone (yellow). (3) Electronic parameters: The presence of a white region near the bond between the 3-phenyl ring and its *para* substituent is compatible with the favorable influence of σ identified in the 2D-QSAR model. The greater the value of σ for a *para* substituent, the higher the positive atomic charge on the *para* aromatic carbon (C4'). Thus the increase of this atomic charge is reflected by a positive (white) zone in the CoMFA models. The magenta zone is probably associated with an additional anchor point within the MAO-B active site. However, its exact nature (electrostatic interaction or hydrogen bond) is not yet established.

3D-QSAR Study with the Combined Series A and B. Compiling series A and B (39 compounds with useable activities), three models based on the alignments described above, were derived. As reported in Table 6, a single field alone yields a satisfactory q^2 in a number of cases (models D1, D3, E1, E3, F3). Again the contribution of the lipophilicity field proved important in all models with two fields (models D5, D6, E5, E6, F5, F6). The best models were obtained with alignments 1 or 3 using the three fields (models D7, F7), with model D7 having the best predictive quality of all ($q^2 = 0.78$). However, model F7 which is almost as good was chosen as the final one since the orientation of *ortho*

and *meta* of minimized compounds (alignment 1) was almost random, which renders the results of D7 less clear.

The graphical representation of model F7 (Figure 4b) shows that all the favorable and unfavorable zones of the three fields occupy well-distinct sectors in space and are therefore not intercorrelated. As with model C7, a bulky lipophilic substituent in the *para* or *meta* position of the 3-phenyl ring can make a favorable steric contribution (green zone), whereas an *ortho* substituent decreases MAO-B inhibitory activity (red zone). Electron-withdrawing substituents in *para* and *meta* positions are doubly favorable for activity, since they induce a favorable region of high electron density close to the substituents themselves (magenta zone) and a favorable region of electron deficiency close to the 4'-carbon (white zone). A region of favorable hydrophilic contribution is seen above and below ring C of the indenopyridazine system (cyan zone) presumably expressing the influence of substituents in the 4 position. Indeed, lipophilic 4-substituents decrease MAO-B inhibitory activity, whereas polar 4-substituents increase it. Model F7 is quite satisfactory in predicting the IC_{50} of compound **16** ($pIC_{50estlm} = 4.85/pIC_{50pred} = 4.69$) and compound **56** ($pIC_{50estlm} = 6.16/pIC_{50pred} = 5.80$).

The statistical results and the combined steric, electrostatic, and lipophilic contributions in models D7, E7, and F7 are in agreement with the CoMFA study of series B. Indeed, models D7, E7, and F7 do not contain important additional information relative to models A7, B7, and C7 for the 3-phenyl ring and its substituents, but they alone explore variations around ring C of the indenopyridazine ring. In contrast, this study did not generate any information regarding substitution of rings A and B.

Conclusion

5*H*-Indeno[1,2-*c*]pyridazin-5-ones are shown here to be competitive, reversible MAO inhibitors with a relatively high selectivity for MAO-B. The most potent compound (**51**) is comparable to some of the best inhibitors known to date, e.g., lazabemide ($IC_{50} = 30$ nM)²¹ and some time-dependent inhibitors of the oxadiazol series (where the most active compound has an IC_{50} of 1.4 nM after 60 min).¹⁵ Congruent 2D- and 3D-QSAR analyses allowed to gain insight into the key structural features governing MAO-B inhibitory activity of indenopyridazines.

Experimental Section

Chemistry. Melting points were determined by the capillary method on a Gallekamp MFB 595 010M electrothermal apparatus and are uncorrected. Elemental analyses were performed on a Carlo Erba 1106 analyzer; for C, H, and N the results agreed to within $\pm 0.40\%$ of the theoretical values. IR spectra were recorded using potassium bromide disks on a Perkin-Elmer 283 spectrophotometer. Only the most significant IR absorption bands are listed. ¹H-NMR spectra were recorded at 300 MHz on a Bruker 300 instrument for the indeno[1,2-*c*]pyridazin-5-one derivatives and at 90 MHz on a 390 Varian spectrometer for intermediate aldol adducts (Scheme 1). Chemical shifts are expressed in δ (ppm) and the coupling constants J in hertz (Hz). The following abbreviations are used, s, singlet; d, doublet; t, triplet; q, quartet; m, multiplet; dd, double doublet; dt, double triplet; td, triple doublet; qd, quadruple doublet; tdd, triple double doublet; br, broad signal. Signals due to OH and NH protons were located by deuterium exchange with D₂O.

IR and $^1\text{H-NMR}$ spectra were fully consistent with the proposed structures. The synthesis of compounds **1**, **4**, **7**, **12**, **25**, **34**, **57**; **8**, **9**, **15**, **18**, **19**, **21**, **23**, **24**, **28–30**, **41**, **43–45**, **47**, **50**, **56**, **58**; and **2**, **3**, **5**, **6**, **10**, **14**, **16**, **17**, **20**, **31**, **39**, **53**, **55** has been described by Kneubühler et al.¹⁷ and Carotti et al.¹¹

Synthesis of 5H-Indeno[1,2-c]pyridazin-5-ones 33, 36, 40, 42, 46, 49, 51, 52, and 65. General One-Pot Procedure (Methods A and B). A solution of ninhydrin (1.78 g, 10 mmol) and a suitable ketone (10 mmol) in 50 mL of glacial AcOH was heated to reflux until a check by TLC showed the complete disappearance of the starting materials (normally 1–3 h). The reaction mixture was allowed to cool to room temperature, and then 0.74 mL (15 mmol) of hydrazine hydrate (98%) was slowly added under magnetic stirring (method A). Such an addition could also be done after a 1-to-4 dilution with acetonitrile (method B). The completion of the reaction was normally obtained within 2–4 h. Title compounds were separated as solids from the reaction mixture, either directly or, if necessary, upon addition of few drops of water.

3-(3'-Methoxyphenyl)-5H-indeno[1,2-c]pyridazin-5-one (33): method B; yield 41%; mp 159–60 °C, from ethanol; $^1\text{H-NMR}$ (CDCl_3) δ 8.19 (qd, 1H, $J = 7.5, 1.0, 0.8$), 7.99 (s, 1H), 7.87 (qd, 1H, $J = 7.5, 1.2, 0.8$), 7.78 (dd, 1H, $J = 2.6, 2.0$), 7.75 (td, 1H, $J = 7.5, 1.2$), 7.63 (qd, 1H, $J = 8.0, 2.0, 0.9$), 7.57 (td, 1H, $J = 7.5, 1.0$), 7.45 (t, 1H, $J = 8.0$), 7.08 (qd, 1H, $J = 8.0, 2.6, 0.9$), 3.91 (s, 3H); IR (cm^{-1}) 1730, 1415. Anal. ($\text{C}_{18}\text{H}_{12}\text{N}_2\text{O}_2$) C, H, N.

3-(3'-Methoxy-4'-hydroxyphenyl)-5H-indeno[1,2-c]pyridazin-5-one (36): method B; yield 24%; mp 253–4 °C dec, from ethanol; $^1\text{H-NMR}$ (CDCl_3) δ 8.16 (dd, 1H, $J = 7.7, 1.0$), 7.96 (s, 1H), 7.92 (d, 1H, $J = 2.0$), 7.85 (dd, 1H, $J = 7.7, 1.0$), 7.74 (td, 1H, $J = 7.7, 1.0$), 7.55 (td, 1H, $J = 7.7, 1.0$), 7.54 (dd, 1H, $J = 8.3, 2.0$), 7.48 (d, 1H, $J = 8.3$), 5.91 (s, 1H, D_2O exchange), 4.01 (s, 3H); IR (cm^{-1}) 3180 (br), 1725, 1415. Anal. ($\text{C}_{18}\text{H}_{12}\text{N}_2\text{O}_3$) C, H, N.

3-(3'-Fluorophenyl)-5H-indeno[1,2-c]pyridazin-5-one (40): method A; yield 64%; mp 215–6 °C, from ethanol/dioxane (95:5); $^1\text{H-NMR}$ (CDCl_3) δ 8.17 (dd, 1H, $J = 7.1, 1.0$), 7.95 (s, 1H), 7.88 (qd, 1H, $J = 8.3, 2.5, 1.8$), 7.91–7.81 (m, 2H), 7.73 (td, 1H, $J = 7.1, 1.0$), 7.56 (td, 1H, $J = 7.4, 1.0$), 7.49 (td, 1H, $J = 8.3, 6.2$), 7.21 (tdd, 1H, $J = 8.3, 2.5, 1.0$); IR (cm^{-1}) 1720, 1430, 1410. Anal. ($\text{C}_{17}\text{H}_9\text{FN}_2\text{O}$) C, H, N.

3-(3',4'-Difluorophenyl)-5H-indeno[1,2-c]pyridazin-5-one (42): method A; yield 63%; mp 260–1 °C, from ethanol/dioxane (90:10); $^1\text{H-NMR}$ (CDCl_3) δ 8.19 (dd, 1H, $J = 7.6, 0.9$), 8.05 (qd, 1H, $J = 11.2, 7.5, 2.2$), 7.95 (s, 1H), 7.87 (dd, 1H, $J = 7.6, 0.9$), 7.84 (m, 1H), 7.76 (td, 1H, $J = 7.6, 0.9$), 7.58 (td, 1H, $J = 7.6, 0.9$), 7.34 (dt, 1H, $J = 9.8, 8.5$); IR (cm^{-1}) 1730, 1430, 1415. Anal. ($\text{C}_{17}\text{H}_8\text{F}_2\text{N}_2\text{O}$) C, H, N.

3-(3',5'-Dichlorophenyl)-5H-indeno[1,2-c]pyridazin-5-one (46): method A; yield 76%; mp 291–2 °C, from ethanol; $^1\text{H-NMR}$ (CDCl_3) δ 8.21 (qd, 1H, $J = 7.5, 1.1, 0.8$), 8.02 (d, 2H, $J = 1.9$), 7.94 (s, 1H), 7.87 (qd, 1H, $J = 7.5, 1.2, 0.8$), 7.76 (td, 1H, $J = 7.5, 1.2$), 7.58 (td, 1H, $J = 7.5, 1.1$), 7.51 (t, 1H, $J = 1.9$); IR (cm^{-1}) 1705, 1400. Anal. ($\text{C}_{17}\text{H}_8\text{Cl}_2\text{N}_2\text{O}$) C, H, N.

3-[2'-(Trifluoromethyl)phenyl]-5H-indeno[1,2-c]pyridazin-5-one (49): method B; yield 23%; mp 180–1 °C, from ethanol; $^1\text{H-NMR}$ (CDCl_3) δ 8.22 (dd, 1H, $J = 7.7, 1.0$), 7.87 (dd, 1H, $J = 7.7, 1.0$), 7.84 (dd, 1H, $J = 8.4, 1.1$), 7.76 (td, 1H, $J = 7.7, 1.0$), 7.70 (s, 1H), 7.67 (dd, 1H, $J = 6.5, 1.4$), 7.63–7.55 (m, 3H); IR (cm^{-1}) 1710, 1410, 1310. Anal. ($\text{C}_{18}\text{H}_9\text{F}_3\text{N}_2\text{O}$) C, H, N.

3-[4'-(Trifluoromethyl)phenyl]-5H-indeno[1,2-c]pyridazin-5-one (51): method A; yield 79%; mp 270–1 °C, from ethanol/dioxane (90:10); $^1\text{H-NMR}$ (CDCl_3) δ 8.25 (d, 2H, $J = 8.1$), 8.21 (dt, 1H, $J = 7.5, 1.0$), 8.02 (s, 1H), 7.88 (dt, 1H, $J = 7.5, 1.0$), 7.81 (d, 2H, $J = 8.1$), 7.76 (td, 1H, $J = 7.5, 1.0$), 7.59 (td, 1H, $J = 7.5, J = 1.0$); IR (cm^{-1}) 1725, 1420, 1330. Anal. ($\text{C}_{18}\text{H}_9\text{F}_3\text{N}_2\text{O}$) C, H, N.

3-[3',5'-Bis(trifluoromethyl)phenyl]-5H-indeno[1,2-c]pyridazin-5-one (52): method B; yield 39%; mp 214–5 °C, from ethanol; $^1\text{H-NMR}$ (CDCl_3) δ 8.61 (s, 2H), 8.22 (dd, 1H, $J = 7.7, 0.8$), 8.06 (s, 1H), 8.03 (s, 1H), 7.90 (dd, 1H, $J = 7.7, 0.9$), 7.79 (td, 1H, $J = 7.7, 0.9$), 7.61 (td, 1H, $J = 7.7, 0.8$); IR (cm^{-1}) 1720, 1390, 1280. Anal. ($\text{C}_{19}\text{H}_8\text{F}_6\text{N}_2\text{O}$) C, H, N.

3-[3'-(Trifluoromethyl)phenyl]-7-methoxy-5H-indeno[1,2-c]pyridazin-5-one (65): method A; yield 60%; mp 214–5 °C, from ethanol; $^1\text{H-NMR}$ (CDCl_3) δ 8.40 (s, 1H), 8.30 (d, 1H, $J = 7.7$), 7.98 (s, 1H), 7.81 (d, 1H, $J = 8.4$), 7.78 (d, 1H, $J = 7.7$), 7.69 (t, 1H, $J = 7.7$), 7.67 (d, 1H, $J = 2.3$), 7.03 (dd, 1H, $J = 8.4, 2.3$), 4.01 (s, 3H); IR (cm^{-1}) 1720, 1405, 1330. Anal. ($\text{C}_{19}\text{H}_{11}\text{F}_3\text{N}_2\text{O}_2$) C, H, N. The 8-methoxy positional isomer was detected by HPLC-MS (5%).

Synthesis of Aldol Adducts 22a, 35a, 48a, 54a, 59a, 60a, 61a, and 62a. The preparation of the title compounds followed the described one-pot procedure up to the disappearance of starting reagents ninhydrin and ketones (TLC check). The workup method was as follows. (i) Adduct **22a**: the solid product, which precipitated from the reaction mixture upon cooling, was collected by filtration and recrystallized. (ii) Adducts **35a**, **48a**, **54a**, **59a**, **60a**, **61a**, and **62a**: the reaction mixture was evaporated to dryness under vacuum, and the solid residue was purified by crystallization (**35a**, **48a**, **54a**, **61a**, **62a**) or flash chromatography on silica gel using CHCl_3 (**59a**, **60a**) as eluent. Reaction yields and physicochemical and spectroscopic data of the isolated aldol adducts are listed in Table 6.

Synthesis of 5H-Indeno[1,2-c]pyridazin-5-ones 22, 35, 48, 54, 59, 60, 61, and 62 (Method C). Hydrazine hydrate (98% (0.50 mL, 10 mmol)) was added under magnetic stirring to the solution of an aldol adduct (10 mmol) in anhydrous EtOH (100–200 mL) containing 0.1 mL of CF_3COOH . The yellow solid which was formed within 1–3 h was collected by filtration and recrystallized.

3-(2'-Carboxyethyl)-5H-indeno[1,2-c]pyridazin-5-one (22): yield 72%; mp 200–1 °C dec, from ethanol; $^1\text{H-NMR}$ (acetone- d_6) δ 12.25 (br, 1H, D_2O exchange), 8.05 (dd, 1H, $J = 8.3, 1.0$), 7.82 (dd, 1H, $J = 8.3, 1.0$), 7.80 (td, 1H, $J = 8.3, J = 1.0$), 7.78 (s, 1H), 7.63 (td, 1H, $J = 8.3, J = 1.0$), 3.21 (t, 2H, $J = 7.5$), 2.80 (t, 2H, $J = 7.5$); IR (cm^{-1}) 3020 (br), 1730, 1710, 1425, 1415. Anal. ($\text{C}_{14}\text{H}_{10}\text{N}_2\text{O}_3$) C, H, N.

3-(3',4'-Dimethoxyphenyl)-5H-indeno[1,2-c]pyridazin-5-one (35): yield 82%; mp 257–8 °C, from THF/ethanol (50:50); $^1\text{H-NMR}$ ($\text{DMSO}-d_6$) δ 8.42 (s, 1H), 8.11 (dt, 1H, $J = 7.4, 1.0$), 7.92–7.80 (m, 4H), 7.66 (td, 1H, $J = 7.4, 1.0$), 7.12 (d, 1H, $J = 8.4$), 3.88 (s, 3H), 3.84 (s, 3H); IR (cm^{-1}) 1720, 1420. Anal. ($\text{C}_{19}\text{H}_{14}\text{N}_2\text{O}_3$) C, H, N.

3-(4'-Bromophenyl)-5H-indeno[1,2-c]pyridazin-5-one (48): yield 90%; mp 261–2 °C, from ethanol; $^1\text{H-NMR}$ (CDCl_3) δ 8.18 (dt, 1H, $J = 7.5, 1.0, 1.0$), 8.00 (m, 2H), 7.96 (s, 1H), 7.86 (qd, 1H, $J = 7.5, 1.2, 1.0$), 7.75 (td, 1H, $J = 7.5, 1.2$), 7.67 (m, 2H), 7.56 (td, 1H, $J = 7.5, 1.0$); IR (cm^{-1}) 1725, 1415. Anal. ($\text{C}_{17}\text{H}_9\text{BrN}_2\text{O}$) C, H, N.

3-(4'-Cyanophenyl)-5H-indeno[1,2-c]pyridazin-5-one (54): yield 93%; mp 298–9 °C, from ethanol; $^1\text{H-NMR}$ (CDCl_3) δ 8.24 (m, 2H), 8.20 (dt, 1H, $J = 7.5, 1.1$), 8.01 (s, 1H), 7.88 (dt, 1H, $J = 7.5, 1.1$), 7.84 (m, 2H), 7.77 (td, 1H, $J = 7.5, 1.1$), 7.59 (td, 1H, $J = 7.5, 1.1$); IR (cm^{-1}) 2220, 1720, 1415. Anal. ($\text{C}_{18}\text{H}_9\text{N}_3\text{O}$) C, H, N.

3-(4'-Acetylphenyl)-5H-indeno[1,2-c]pyridazin-5-one (59): yield 95%; mp 256–7 °C, from ethanol; $^1\text{H-NMR}$ (CDCl_3) δ 8.24 (m, 2H), 8.21 (m, 1H), 8.13 (m, 2H), 8.05 (s, 1H), 7.88 (m, 1H), 7.77 (td, 1H, $J = 7.6, 1.2$), 7.59 (td, 1H, $J = 7.6, 1.2$), 2.68 (s, 3H); IR (cm^{-1}) 1730, 1670, 1415. Anal. ($\text{C}_{19}\text{H}_{12}\text{N}_2\text{O}_2$) C, H, N.

3-(4'-Acetamidophenyl)-5H-indeno[1,2-c]pyridazin-5-one (60): yield 76%; mp 338–9 °C, from THF; $^1\text{H-NMR}$ (CDCl_3) δ 10.25 (br, 1H, D_2O exchange), 8.18 (dt, 1H, $J = 7.6, 1.0$), 8.12 (m, 2H), 7.97 (s, 1H), 7.85 (dt, 1H, $J = 7.6, 1.0$), 7.74 (td, 1H, $J = 7.6, J = 1.0$), 7.70 (m, 2H), 7.55 (td, 1H, $J = 7.6, 1.0$), 2.13 (s, 3H); IR (cm^{-1}) 3380, 1720, 1690, 1595, 1415. Anal. ($\text{C}_{19}\text{H}_{13}\text{N}_3\text{O}_2$) C, H, N.

3-(4'-Butoxyphenyl)-5H-indeno[1,2-c]pyridazin-5-one (61): yield 72%; mp 178–9 °C, from ethanol; $^1\text{H-NMR}$ (CDCl_3) δ 8.15 (dt, 1H, $J = 7.5, 1.1$), 8.07 (m, 2H), 7.92 (s, 1H), 7.83 (dt, 1H, $J = 7.5, 1.1$), 7.72 (td, 1H, $J = 7.5, 1.1$), 7.53 (td, 1H, $J = 7.5, 1.1$), 7.02 (m, 2H), 4.03 (t, 2H, $J = 6.5$), 1.79 (m, 2H), 1.49 (m, 2H), 0.98 (t, 3H, $J = 6.5$); IR (cm^{-1}) 1730, 1410. Anal. ($\text{C}_{21}\text{H}_{18}\text{N}_2\text{O}_2$) C, H, N.

3-(4'-Piperidinylphenyl)-5H-indeno[1,2-c]pyridazin-5-one (62): yield 20%; mp 224–5 °C, from ethanol; $^1\text{H-NMR}$

(CDCl₃) δ 8.15 (dt, 1H, J = 7.6, 1.1), 8.05 (m, 2H), 7.92 (s, 1H), 7.83 (qd, 1H, J = 7.6, 1.2, 1.1), 7.72 (td, 1H, J = 7.6, 1.2), 7.52 (td, 1H, J = 7.6, 1.1), 7.01 (m, 2H), 3.33 (m, 4H), 1.69 (m, 6H); IR (cm⁻¹) 1720, 1410. Anal. (C₂₂H₁₉N₃O) C, H, N.

3-Phenyl-4-(ethoxycarbonyl)-5H-indeno[1,2-c]pyridazin-5-one (11). To a solution of ninhydrin (1.78 g, 10 mmol) in dimethoxyethane (25 mL) on molecular sieves (3 Å), kept at room temperature over 1 day, was added an equimolar amount of ethyl benzoylacetate. The resulting mixture was left to stand at room temperature for 3 days and then filtered and diluted to ca. 0.025 M concentration with anhydrous ethanol (375 mL). An equimolar amount of hydrazine monohydrate was added, under magnetic stirring, and after 3 h, the solution obtained was evaporated to dryness under vacuum and the residue purified by flash chromatography using hexane/ethyl acetate (80:20) as eluent: yield 20%; mp 113–4 °C, from ethanol; ¹H-NMR (90 MHz, CDCl₃) δ 8.23 (d, 1H, J = 7), 7.93–7.33 (m, 8H), 4.41 (q, 2H, J = 7), 1.27 (t, 3H, J = 7); IR (cm⁻¹) 1740, 1730, 1395. Anal. (C₂₀H₁₄N₂O₃) C, H, N.

3-Benzoyl-5H-indeno[1,2-c]pyridazin-5-one (13). 3-Benzoyl-5H-indeno[1,2-c]pyridazin-5-one (HCA) (272 mg, 1 mmol) in acetic acid (2 mL) was refluxed with 130 mg (1.3 mmol) of chromium(VI) oxide for 2 h. After cooling the mixture was diluted with water (8 mL), extracted with CHCl₃, and evaporated under vacuum. The residue was purified by flash chromatography using CHCl₃ as eluent: yield 94%; mp 168–9 °C dec, from ethanol; ¹H-NMR (CDCl₃) δ 8.27 (s, 1H), 8.27–8.21 (m, 3H), 7.91 (td, 1H, J = 7.5, 1.1), 7.79 (td, 1H, J = 7.5, 1.1), 7.80–7.60 (m, 2H), 7.56–7.48 (m, 2H); IR (cm⁻¹) 1720, 1660, 1410. Anal. (C₁₈H₁₀N₂O₂) C, H, N.

13H-Benz[h]indeno[1,2-c]cinnolin-13-one (26). 11,12-Dihydro-13H-benz[h]indeno[1,2-c]cinnolin-13-one (HCA) (284 mg, 1 mmol) in dioxane (5 mL) was refluxed with 227 mg (1.3 mmol) of 2,3-dichloro-5,6-dicyano-1,4-benzoquinone over 1.5 h. After cooling the solvent was evaporated, and the residue was purified by flash chromatography on silica gel using CHCl₃/ethyl acetate (90:10) as eluent: yield 90%; mp 261–2 °C, from ethanol; ¹H-NMR (CDCl₃) δ 9.38 (m, 1H), 8.41 (d, 1H, J = 9.0), 8.14 (dt, 1H, J = 7.3, 1.2), 7.95 (d, 1H, J = 9.0), 7.86–7.67 (m, 4H), 7.65 (td, 1H, J = 7.5, 1.2), 7.45 (td, 1H, J = 7.5, 1.1); IR (cm⁻¹) 1720, 1400. Anal. (C₁₉H₁₀N₂O) C, H, N.

11H-Indeno[1,2-c]cinnolin-11-one (27). 1,2,3,4-Tetrahydro-11H-indeno[1,2-c]cinnolin-11-one¹¹ (236 mg, 1 mmol) in dioxane (10 mL) was refluxed with 522 mg (2.3 mmol) of 2,3-dichloro-5,6-dicyano-1,4-benzoquinone for 2.5 h. After cooling, the mixture was concentrated, and the residue was purified by flash chromatography on silica gel using CHCl₃/ethyl acetate (90:10) as eluent: yield 12%; mp 285–6 °C dec, from ethanol; ¹H-NMR (CDCl₃) δ 8.65 (m, 1H), 8.50 (m, 1H), 8.17 (dt, 1H, J = 7.6, 1.0), 7.88–7.76 (m, 2H), 7.75 (qd, 1H, J = 7.6, 1.1, 1.0), 7.65 (td, 1H, J = 7.6, 1.2), 7.45 (td, 1H, J = 7.6, 1.0); IR (cm⁻¹) 1720, 1390. Anal. (C₁₅H₈N₂O) C, H, N.

3-(2'-Methoxyphenyl)-5H-indeno[1,2-c]pyridazin-5-one (32). 2'-Methoxyacetophenone (300 mg, 2 mmol) and 356 mg (2 mmol) of ninhydrin were refluxed in acetic acid (4 mL) for 2 h. The solution was cooled, and the solid obtained was collected and washed with diethyl ether. This crude aldol adduct was dissolved in THF (40 mL), and 0.1 mL (2 mmol) of hydrazine monohydrate was added under magnetic stirring. After 2 h the mixture was evaporated under vacuum and the residue was purified by flash chromatography on silica gel using CHCl₃ as eluent: yield 24%; mp 162–3 °C, from CHCl₃/hexane; ¹H-NMR (CDCl₃) δ 8.16 (dt, 1H, J = 7.6, 0.9), 8.14 (s, 1H), 7.96 (dd, 1H, J = 7.6, 1.8), 7.83 (qd, 1H, J = 7.6, 1.2, 0.9), 7.71 (td, 1H, J = 7.6, 1.2), 7.53 (td, 1H, J = 7.6, 0.9), 7.46 (qd, 1H, J = 8.3, 7.6, 1.8), 7.11 (td, 1H, J = 7.6, 1.0), 7.02 (dd, 1H, J = 8.3, J = 1.0), 3.88 (s, 3H); IR (cm⁻¹) 1730, 1410. Anal. (C₁₈H₁₂N₂O₂) C, H, N.

3-(3'-Aminophenyl)-5H-indeno[1,2-c]pyridazin-5-one (37). A solution of crude 3-[3'-(*N*-carbobenzoxyamino)phenyl]-5H-indeno[1,2-c]pyridazin-5-one (814 mg, 2 mmol), prepared according to method B from *N*-carbobenzoxy-3'-aminoacetophenone, was refluxed over 1.5 h in 20 mL of aqueous HBr/acetic acid (50:50). The mixture was cooled at room temperature and made basic with KOH, and the red solid obtained was separated by filtration and purified by flash chromatography

on silica gel using ethyl acetate/hexane (50:50) as eluent: yield 61%; mp 237–8 °C, from ethanol; ¹H-NMR (CDCl₃) δ 8.18 (m, 1H), 7.95 (s, 1H), 7.85 (m, 1H), 7.73 (td, 1H, J = 7.2, 1.0), 7.55 (m, 1H), 7.54 (m, 1H), 7.41 (dt, 1H, J = 7.7, 1.1), 7.31 (t, 1H, J = 7.7), 6.83 (qd, 1H, J = 7.7, 2.7, 1.1), 3.87 (br, 2H, D₂O exchange); IR (cm⁻¹) 3305, 3210, 1730 1635, 1415. Anal. (C₁₇H₁₁N₃O) C, H, N.

3-(4'-Aminophenyl)-5H-indeno[1,2-c]pyridazin-5-one (38). Compound 38 was synthesized as the isomeric compound 37 from 3-[4'-(*N*-carbobenzoxyamino)phenyl]-5H-indeno[1,2-c]pyridazin-5-one. The red solid obtained was purified by crystallization: yield 58%; mp 295–6 °C, from butanol; ¹H-NMR (CDCl₃) δ 8.15 (d, 1H, J = 7.7), 7.98 (m, 2H), 7.91 (s, 1H), 7.83 (d, 1H, J = 7.7), 7.72 (t, 1H, J = 7.7), 7.53 (t, 1H, J = 7.7), 6.79 (m, 2H), 3.99 (br, 2H, D₂O exchange); IR (cm⁻¹) 3410, 3390, 1730, 1630 1610, 1425. Anal. (C₁₇H₁₁N₃O) C, H, N.

3-(Trifluoromethyl)-5H-indeno[1,2-c]pyridazin-5-one (64). Ethyl 4,4,4-trifluoroacetate (0.24 mL, 2 mmol) and 356 mg (2 mmol) of ninhydrin were refluxed in acetic acid (4 mL). After 1.5 h the solution was diluted with acetonitrile (12 mL) and 0.15 mL (3 mmol) of hydrazine monohydrate was added. The yellow solid formed was filtered and dissolved in 4 mL of trifluoroacetic acid. After stirring at room temperature for 4 h, the solution was evaporated under vacuum, and the solid residue was purified by crystallization: yield 20%; mp 157–8 °C, from CHCl₃/hexane; ¹H-NMR (CDCl₃) δ 8.24 (m, 1H), 7.92 (m, 1H), 7.89 (s, 1H), 7.79 (td, 1H, J = 7.0, 1.0), 7.64 (td, 1H, J = 7.0, 1.0); IR (cm⁻¹) 1720, 1360, 1290. Anal. (C₁₂H₅F₃N₂O) C, H, N.

3-[3'-(Trifluoromethyl)phenyl]-7-hydroxy-5H-indeno[1,2-c]pyridazin-5-one (66). 65 (712 mg, 2 mmol) was refluxed in 10 mL of aqueous HBr (47%)/acetic acid (50:50) for 2 h. The mixture was filtered and extracted with CHCl₃. The organic layer was evaporated under vacuum, and the residue was purified by flash chromatography on silica gel using CHCl₃/methanol (95:5) as eluent: yield 25%; mp 351–2 °C, from ethanol; ¹H-NMR (DMSO-*d*₆) δ 11.34 (br, 1H, D₂O exchange), 8.59 (s, 1H), 8.57 (d, 1H, J = 8.0), 8.50 (s, 1H), 7.92 (d, 1H, J = 8.0), 7.81 (t, 1H, J = 8.0), 7.77 (d, 1H, J = 8.5), 7.44 (d, 1H, J = 2.2), 6.99 (dd, 1H, J = 8.5, 2.2); IR (cm⁻¹) 3200 (br), 1705, 1475, 1340. Anal. (C₁₈H₉F₃N₂O₂) C, H, N.

Preparation of Rat Brain Mitochondria. Rat brain mitochondria were isolated according to the method of Clark²² modified by Walther et al.²³ For further details, see Thull et al.²⁴ The protein content of the washed mitochondrial fraction was determined according to the procedure of Lowry²⁵ with bovine serum albumin as a standard.

MAO Inhibition. The method of Weissbach²⁶ was modified in order to measure inhibitory activities.²⁴ IC₅₀ values were calculated from a hyperbolic equation described elsewhere.²⁴ Time dependence was tested by preincubating for 5 and 15 min at 37 °C and at a single concentration of the inhibitor. Reversibility was demonstrated by measuring the degree of inhibition in the presence of a higher substrate concentration (540 μ M).

Incubations were carried out at pH = 7.4 (Na₂HPO₄/KH₂PO₄ isotonicized with KCl) at 37 °C. The mitochondrial suspension was set to a final protein concentration of 1.0 mg/mL. The mitochondria were preincubated at 37 °C for 5 min with clorgyline (250 nM) or selegiline (250 nM) to test MAO-B or MAO-A activity, respectively. The inhibitor under study was solubilized in DMSO, added to give a final DMSO concentration of 5% (v/v), and further incubated for 5 min. Preliminary experiments had verified that DMSO at this concentration does not affect MAO activity. The nonselective substrate kynuramine is deaminated by MAO to an aldehyde that spontaneously cyclizes to 4-hydroxyquinoline. Formation of the latter was monitored continuously at 314 nm using a Kontron UVIKON 941 spectrophotometer (Kontron AG, Basel, Switzerland). Incubations were then carried out with a substrate concentration of K_M (K_M = 90 μ M for MAO-A, 60 μ M for MAO-B) without inhibitor or with different inhibitor concentrations.

QSAR Study. Multilinear regression and cluster analysis were carried out with TSAR 2.1 software (Oxford Molecular,

Oxford, U.K.), and PLS analysis was performed using the QSAR module in SYBYL 6.04 software (Tripos Assoc., St. Louis, MO). Both programs were run on Silicon Graphics Personal Iris 4D-35 and Silicon Graphics Indigo R4000 workstations. The σ values were collected from standard compilations.^{19,27} If not available, the F , R , and σ parameters for *ortho* substituents were calculated according to Williams and Norrington.²⁸

CoMFA (3D-QSAR) Study. Molecular models of the IP analogs listed in Tables 2 and 3 were constructed using SYBYL 6.04 software (Tripos Assoc., St. Louis, MO) running on Silicon Graphics Personal Iris 4D-35 and Silicon Graphics Indigo R4000 workstations. The geometry of each molecule was minimized using the standard Tripos force field²⁹ including the electrostatic energy term calculated with the Gasteiger-Marsili atomic charges.³⁰ From a conformational analysis performed with the systematic search option, the lowest energy minimum was selected for each compound and minimized.

The CoMFA studies were carried out by using the QSAR module of SYBYL version 6.04. Default settings²⁰ were used in the analyses, except for the option "drop-electrostatic" which was set to "no". The grid size had a resolution of 1.5 Å. As a third field, the Molecular Lipophilicity Potential (MLP) was used.³¹ Only those compounds for which an IC₅₀ value could be determined (i.e., 39 compounds in Tables 2 and 3) were used in the analyses. Only models with $q^2 > 0.4$ were considered as significant. To avoid reducing the training set, we took as test set the two compounds (**16** and **56**) which had a degree of inhibition larger than 25% at their maximum solubility, thus allowing their IC₅₀ values to be calculated with reasonable confidence by hyperbolic extrapolation.

Acknowledgment. B.T. and P.A.C. are grateful to the Swiss National Science Foundation for support. The Italian authors gratefully acknowledge support from MURST and CNR (Rome, Italy).

References

- Sandler, M. Monoamine oxidase inhibitor efficacy in depression and the "cheese effect". *Psychol. Med.* **1981**, *11*, 455–458.
- Kyburz, E. New developments in the field of MAO inhibitors. *Drug News Perspect.* **1990**, *3*, 592–599.
- Youdim, M. B. H.; Finberg, J. P. M. New directions in monoamine oxidase A and B selective inhibitors and substrates. *Biochem. Pharmacol.* **1991**, *41*, 155–162.
- Cesura, A. M.; Pletscher, A. The new generation of monoamine oxidase inhibitors. In *Progress in Drug Research*, Vol. 38; Jucker, E., Ed.; Birkhäuser Verlag: Basel, Switzerland, 1992; pp 171–297.
- DaPrada, M.; Kettler, R.; Haefely, W. E. Some basic aspects of reversible inhibitors of monoamine oxidase-A. *Acta Psychiatr. Scand.* **1990**, *360* (Suppl.), 7–12.
- Haefely, W. E.; Burkard, W. P.; Cesura, A. M.; Kettler, R.; Lorez, H. P.; Martin, J. R.; Richards, J. G.; Scherschlicht, R.; DaPrada, M. Biochemistry and pharmacology of moclobemide, a prototype RIMA. *Psychopharmacology* **1992**, *106*, 6–14.
- McDonald, I. A.; Bey, P.; Palfreyman, M. G. Monoamine oxidase inhibitors. In *Design of Enzyme Inhibitors as Drugs*; Sandler, M., Smith, H. J., Eds.; Oxford University Press: Oxford, U.K., 1989; pp 227–243.
- Tipton, K. F.; Fowler, C. J. The kinetics of monoamine oxidase inhibitors in relation to their clinical behaviour. In *Monoamine Oxidase and Disease; Prospects for Therapy with Reversible Inhibitors*; Tipton, K. F., Dostert, P., Strolin Benedetti, M., Eds.; Academic Press: London, U.K., 1984; pp 27–40.
- Heinisch, G.; Kopelent-Frank, H. Pharmacologically active pyridazine derivatives. In *Progress in Medicinal Chemistry*, Vol. 29; Ellis, G. P., Luscombe, D. K., Eds.; Elsevier: Amsterdam, The Netherlands, 1992; pp 141–167.
- Mazouz, F.; Lebreton, L.; Milcent, R.; Burstein, C. Inhibition of monoamine oxidase types A and B by 2-aryl-4H-1,3,4-oxadiazol-5(6H)-one derivatives. *Eur. J. Med. Chem.* **1988**, *23*, 441–451.
- Carotti, A.; Carta, A.; Campagna, F.; Altomare, C.; Casini, G. An efficient route to biologically active 5H-indeno[1,2-c]-pyridazin-5-ones. *Farmaco* **1993**, *48*, 137–141.
- Carotti, A.; Altomare, C.; Campagna, F.; Carta, V.; Kneubühler, S.; Thull, U. Synthesis and monoamine oxidase inhibitory activity of 5H-indeno[1,2-c]pyridazines. *Abstracts of the 12th International Symposium on Medicinal Chemistry*; Swiss Chemical Society: Basel, Switzerland, 1992; p 304.
- Dixon, C. M.; Park, G. R.; Tarbit, M. H. Characterization of the enzyme responsible for the metabolism of sumatriptan in human liver. *Biochem. Pharmacol.* **1994**, *47*, 1253–1257.
- Mazouz, F.; Lebreton, L.; Milcent, R.; Burstein, C. 5-Aryl-1,3,4-oxadiazol-2(3H)-one derivatives and sulfur analogues as new selective and competitive monoamine oxidase type B inhibitors. *Eur. J. Med. Chem.* **1990**, *25*, 659–671.
- Mazouz, F.; Gueddari, S.; Burstein, C.; Mansuy, D.; Milcent, R. 5-(4-Benzyloxyphenyl)-1,3,4-oxadiazol-2(3H)-one derivatives and related analogues: new reversible, highly potent, and selective monoamine oxidase type B inhibitors. *J. Med. Chem.* **1993**, *36*, 1157–1167.
- Thull, U.; Testa, B. Screening of unsubstituted cyclic compounds as inhibitors of monoamine oxidases. *Biochem. Pharmacol.* **1994**, *47*, 2307–2310.
- Kneubühler, S.; Carta, V.; Altomare, C.; Carotti, A.; Testa, B. Synthesis and monoamine oxidase inhibitory activity of 3-substituted 5H-indeno[1,2-c]pyridazines. *Helv. Chim. Acta* **1993**, *76*, 1954–1963.
- Van de Waterbeemd, H.; Testa, B. The parametrization of lipophilicity and other structural properties in drug design. In *Advances in Drug Research*, Vol. 16; Testa, B., Ed.; Academic Press: London, U.K., 1987; pp 85–225.
- Hansch, C.; Leo, A. *Substituent Constants for Correlation Analysis in Chemistry and Biology*; Wiley: New York, 1979.
- Cramer, R. D.; Patterson, D. E.; Bunce, J. D. Comparative molecular field analysis (CoMFA). 1. Effect of shape on binding of steroids to carrier proteins. *J. Am. Chem. Soc.* **1988**, *110*, 5959–5967.
- DaPrada, M.; Kettler, R.; Keller, H. H.; Cesura, A. M.; Richards, J. G.; Saura Marti, J.; Muggli-Maniglio, D.; Wyss, P. C.; Kyburz, E.; Imhof, R. From moclobemide to Ro 19-6327 and Ro 41-1049: the development of a new class of reversible, selective MAO-A and MAO-B inhibitors. *J. Neural. Transm., Suppl.* **1990**, *29*, 279–292.
- Clark, J. B.; Nicklas, W. J. The metabolism of rat brain mitochondria. *J. Biol. Chem.* **1970**, *245*, 4724–4731.
- Walther, B.; Gherzi-Egea, J.; Minn, A.; Siest, G. Brain mitochondrial cytochrome P-450_{sc}: Spectral and catalytic properties. *Arch. Biochem. Biophys.* **1987**, *254*, 592–596.
- Thull, U.; Kneubühler, S.; Testa, B.; Borges, M. F. M.; Pinto, M. M. M. Substituted xanthenes as selective and reversible monoamine oxidase A (MAO-A) inhibitors. *Pharm. Res.* **1993**, *10*, 1187–1190.
- Lowry, O.; Rosebrough, N.; Farr, A.; Randall, R. Protein measurement with the folin phenol reagent. *J. Biol. Chem.* **1951**, *193*, 265–275.
- Weissbach, H.; Smith, T. E.; Daly, J. W.; Witkop, B.; Udenfriend, S. A rapid spectrophotometric assay of monoamine oxidase based on the rate of disappearance of kynuramine. *J. Biol. Chem.* **1960**, *235*, 1160–1163.
- Perrin, D. D.; Dempsey, B.; Serjeant, E. P. *pK_a Prediction for Organic Acids and Bases*; Chapman and Hall: New York, 1981.
- Williams, S. G.; Norrington, F. E. Determination of positional weighting factors for the Swain and Lupton substituent constants F and R. *J. Am. Chem. Soc.* **1976**, *98*, 508–516.
- Clark, M.; Cramer, R. D.; Van Opdenbosch, N. Validation of the general purpose Tripos 5.2 force field. *J. Comput. Chem.* **1989**, *10*, 982–1012.
- Gasteiger, J.; Marsili, M. Iterative partial equalization of orbital electronegativity: a rapid access to atomic charges. *Tetrahedron* **1980**, *36*, 3219–3222.
- Gaillard, P.; Carrupt, P.-A.; Testa, B.; Boudon, A. Molecular lipophilicity potential, a tool in 3D QSAR: Method and applications. *J. Comput.-Aided Mol. Des.* **1994**, *8*, 83–96.

JM950172K